Groundwater flow under permafrost conditions and talik formation

Klaus-Peter Kröhn
GRS gGmbh, Braunschweig, Niedersachsen, Germany

ABSTRACT

In Germany, the safety of a nuclear waste repository legally needs to be investigated for a period of one million years. During the past million years the whole geographic area of present-day Germany has repeatedly experienced permafrost conditions. This will therefore presumably also happen within the time frame that is relevant for the safety assessment. An integral part of such a safety assessment is the transport of radionuclides with the groundwater in case of a canister failure. This assessment requires knowledge of groundwater flow systems. These, however, undergo fundamental alterations in the event of permafrost formation as the freezing of near surface layers may shield the biosphere from possibly contaminated water in deeper aquifers.

However, taliks connecting surface waters with deeper aquifers are known to exist in permafrost regions and can potentially lead to a concentrated flux of contaminated groundwater to the surface. Unfortunately, the circumstances of their formation and their stability — highly important for the safety assessment — are largely unknown. Insight can be gained through numerical modelling which is why a mathematical model for groundwater flow under permafrost conditions including equations of state and constitutive equations has previously been stringently derived. This model is shortly revisited as a basis for a first thermo-hydraulically coupled numerical model that addresses the beginning of a cold age. This work is intended to create trust in the modelling framework as a starting point for further investigations in the future.

1 INTRODUCTION

The safety of the biosphere against undesirable release of radionuclides from a deep geological repository (DGR) is principally at risk where groundwater can corrode the metallic waste canisters. For a performance assessment of a DGR, it is therefore imperative to know the groundwater flow system over the projected lifetime of the repository. According to the current legislation in Germany, this will be over a period of a million years (Deutscher Bundestag 2017).

Over the past million years, several ice ages have occurred and have brought permafrost conditions all over present-day Germany (see Figure 1). It can therefore be expected that any conceivable DGR in Germany will sooner or later also be subject to these conditions during the coming million years. This is significant because permafrost will have a considerable impact on groundwater flow as ground freezing tends to separate deeper aquifers hydraulically from the surface.

However, it is also known that even under permafrost conditions there are local volumes of unfrozen ground, called taliks. According to van Everdingen (2005), a talik can be defined as “A layer or body of unfrozen ground occurring in a permafrost area due to a local anomaly in thermal, hydrological, hydrogeological, or hydrochemical conditions.”

Large taliks have been documented to hydraulically connecting the surface with deeper unfrozen aquifers (e.g., Burn 2020; cf. right sketch in Figure 2). Van Everdingen (2005) recommends the expression “open talik” for this phenomenon but also other terms can be found in the literature. Note that from this point on the expression “talik” is used synonymously to “open talik”.

Figure 1. Permafrost conditions during the latest ice age (after Vandenberghe and Pissart 1993; Renssen and Vandenberghe 2003).

Open taliks are known to exist below large surface water bodies such as lakes and rivers (Delisle 1998; Keller 1998; SKB 2006). Flow of contaminated waters from a possible leakage in a waste repository could be directed towards such taliks and thus lead to a strongly localized outflow into surface waters (e.g., Johansson 2016; Figure 2). Providing means of radionuclide transport to the biosphere through the permafrost and thereby concentrating the flow from the DGR towards the outlet at the surface makes taliks a key feature in the assessment of a possible exposure of the biosphere to harmful radioactive substances. The mechanisms leading to talik formation must therefore be understood to an adequate level of detail in order to allow for meaningful predictions of groundwater flow and possible subsequent contaminant transport under permafrost conditions.

https://doi.org/10.52381/ICOP2024.228.1

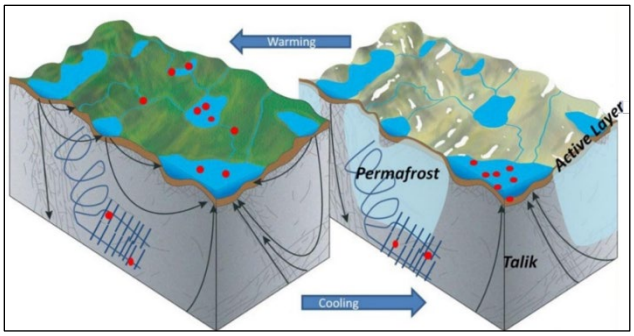

Figure 2. Impact of permafrost on radionuclide migration paths (from Johansson 2016).

Taliks cannot be observed directly, but require laborious field work to document (e.g., Harper et al. 2011). Furthermore, they provide only a snapshot of a long-lasting evolution which makes it hard to identify the relevant circumstances of its occurrence. Numerical modelling is therefore a welcome tool that can be used to understand talik formation without relying on sparse and challenging field data collections. A surprisingly large variety of mathematical formulations can be found in the literature that describe groundwater flow under freezing conditions including ice formation. Some of them have been compiled and discussed by Kröhn (2022) where some formal inconsistencies have been found between assumptions/simplifications during derivation of the balance equations and the ultimately used formulation. Also, no commonly agreed upon set of equations of state (EOS) could be identified as many of the EOS are neither realistic nor appropriate. It was thus concluded that a sound set of formulations should be derived anew to ensure that all relevant processes are properly addressed. Consequently, balance equations, constitutive equations (CE) and EOS were rigorously developed or chosen with care in Kröhn (2022).

The present paper represents the final preparatory step in providing a trustworthy numerical model for groundwater flow under permafrost conditions. This includes formulations for realistic initial and boundary conditions as well as a definition of a model domain including the related hydrogeologic parameters. As granitic rock is presently considered to be a potential host rock for a nuclear waste repository in Germany, the setting at Two Boat Lake in Greenland (e.g., Johansson et al. 2015) where a talik has actually been found (e.g., Harper et al. 2011), is used here as a template. Confidence in the modelling framework is built by having a first model run covering the latest climate cooling period leading to the last glacial maximum. Results are checked for being sensible and consistent. At this stage of development, this first model forms a starting point for future investigations.

2 METHODOLOGY

2.1 Problem definition

2.1.1 Climatic framework

Talik formation may occur either during a change from warmer to colder climates by leaving out an unfrozen “hole” in an otherwise freezing ground, or during a change from cooler to warmer climates by thawing a hole in initially frozen ground.

Presently, talik formation is quite intensively investigated in the framework of a warming cryosphere and is most commonly discussed in the context of thawing (e.g., Parazoo et al. 2018). As Germany is currently ice-free, this appears to be not as relevant in the context of geological storage as the question, where will open taliks remain in an otherwise increasingly freezing ground? It is expected that the freezing dynamics are different from the thawing dynamics since the initial temperature for freezing and thawing scenarios and thus all state variables are different. This difference in dynamics may be enhanced by groundwater flow because heat transport by convection depends on the highly non-linear Soil Freezing Characteristic Curve (SFCC) which in turn entails further non-linearities from the relative permeability. The focus of this article is therefore on a freezing scenario.

2.1.2 Domain

It is assumed that cooling and freezing of water is less complex in lakes than in rivers as rivers show considerably more turbulent water flow than lakes. To keep things as simple as possible, the model presented in this work includes a lake in the domain. This lake is located on top of a granitic formation to have some relation to talik investigations on Greenland (e.g., Johansson et. al. 2015). Porosity and permeability, however, are chosen to coincide with the conditions at the Grimsel Test Site in Switzerland (e.g., Gens et al. 2002) which is also located in crystalline rock.

Axial symmetry is assumed for the hypothetical lake as by (Mackey 1962) to reduce the computational cost. The lake has a maximum depth of 25 m at the centre and a radial extent of 50 m.

2.1.3 Physical framework

Groundwater flow is bounded by lateral no-flow boundaries in the domain. The system is initially hydrostatic. The thermal temperature boundary at the surface is allowed to evolve in time, while a heat flux according to the geothermal gradient is assigned to the base of the profile. The initial thermal conditions depend on the preceding climate which would be a warm period in this case. Within the domain, the temperature distribution is assumed to be in equilibrium with the initial boundary conditions. Modelling begins at the onset of a cold climate.

The lake is approximated in the model as a porous medium with very high values for permeability and porosity, namely 10^{-11} m² and 99 %, respectively, to avoid modelling free water.

2.2 Shaping a model

2.2.1 Mathematical framework

The formulations derived by Kröhn (2022) include the balance equations, the CE as well as their parameters and the EOS considered. They are shortly described and compiled along with a list of processes taken into account and a list of the model assumptions in Appendix A.

Two balance equations are considered. The first one describes mass conservation of water and ice and the second one conservation of heat energy in the three-phase system water, ice, and rock mass allowing for thermo-hydraulically coupled simulations.

Of all the required mathematical formulations, the constitutive equations introduce by far the highest uncertainties in the mathematical framework as they provide a parameterized description of micro-scale properties of the porous medium of interest. Furthermore, they are difficult to measure so that often enough the gut feeling of the modeller decides about the relation and the accompanying parameters to be used. The SFCC and the relative permeability for the present model, for example, are chosen from a comparison of eight related approaches compiled in Kröhn (2022), suggesting the following choice: the water fraction in the pore space S_w is represented by a point symmetric transition curve over the temperature interval -2 °C < T < 0 °C. Relative permeability of the water k_{rw} is taken to be a cubic function of S_w but leaving a residual value of 10^{-6} for $S_w(T)^3 < 10^{-6}$.

Simplified equations of state valid in the temperature range between -20 °C and +20 °C and hydraulic pressures up to 10 MPa had also been developed by Kröhn (2022). Tentative modelling of a changing surface temperature showed, though, that the induced temperature signal went considerably lower than a depth of 1000 m and thereby beyond the limit of 10 MPa (cp. section 2.3). Thus, a new set of EOS expected to be valid up to +60 °C and down to a depth of about 2 km have been derived (Kröhn 2023) and applied here. Evaluation of the modelling results included a check against transgressing the ranges of validity for the EOS (cp. section 2.3).

All these mathematical formulations are realized in the framework of the Code COMSOL Multiphysics.

2.2.4 Thermal setup

Generally, the temperature distribution in the subsurface is influenced by the temperature at the top, by the geothermal heat flux and by the thermal properties of the subsurface. Basically, two mechanisms determine the geothermal heat flux, namely radiogenic and primordial heat, (e.g., Dye, 2012). The former relates to radioactive decay of naturally occurring radioactive elements and the latter to residual heat from planetary accretion. This leads to a complex evolution over geological times. However, over the past million years, the change in heat flux from inner earth amounts only to 0.18% (Loyd et al. 2007) allowing from a rational point of view for the simplification of a constant flux over the period of interest.

According to a recent data survey, heat flux over the area of present-day Germany ranges between 20 and 192 mW/m² (Fuchs et al. 2022b). For the present model, the average of 78 mW/m² (Fuchs et al. 2022a) is adopted for the bottom boundary of the model.

A time-dependent temperature boundary condition is applied at the surface. Climate change as a driver for the evolution of permafrost and thereby of taliks is considered over ten thousand to a hundred thousand years. Data on surface temperature evolution determined from ice cores from Antarctica (Jouzel and Masson-Delmotte 2007) are of great interest when reconstructing climate data. These data are given as differences to a reference value, that dates back to pre-industrial conditions. The data from the last cooling climate are taken as an approximation for the cooling dynamics over present-day Germany which in turn may be a template for future climate changes. Only a reference temperature for pre-industrial Germany thus remains to be determined to construct absolute temperatures for the model top.

Systematic climate measurements in Germany go back to the year 1881 (e.g., Deutscher Wetterdienst (DWD), 2021). At this time, industrial revolution was underway (ERIH 2023). Twelve reconstructions of the temperature evolution of earth's northern hemisphere using "multiple climate proxy records" for the past 1300 years (Solomon et al. 2007) indicate that the temperature was not affected by industrialization until about 1900 (see Figure 3). The wanted reference temperature can thus be established on the basis of the first 20 years of temperature recorded by the DWD. According to data of the Climate Data Center of the DWD (Deutscher Wetterdienst 2023), this value amounts to about +7.6 °C. Note that these measurements refer to a surface air temperature (SAT) at 2 m height above ground.

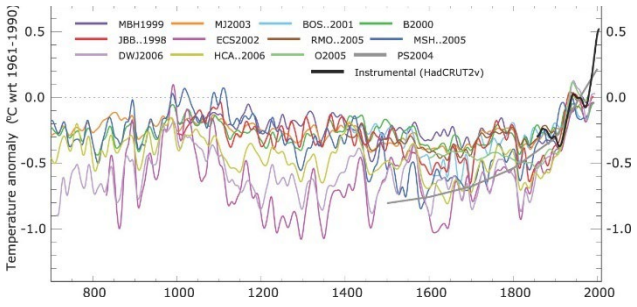

Figure 3. Reconstructions of the temperature anomaly of earth's northern hemisphere (from Solomon et al. 2007).

Daily and seasonal variations of the air temperature may reach down up to about 12 m into the ground (e.g., Deutscher Wetterdienst 2012). However, these few topmost meters can be seen as a temporary storage volume for heat energy that is filled during a warm period and drained again during a cold period. Any net effect of the heat flow fluctuations on the temperature field is attenuated

over space and time. It is therefore assumed that temperature variations between the SAT and the ground temperature at about 12 m depth can be neglected leaving annual average temperatures to be considered in this work. In other words, the SAT can directly be applied as the thermal surface boundary condition for the model. The temperature evolution for the past 250,000 years is adopted accordingly and shown in Figure 4.

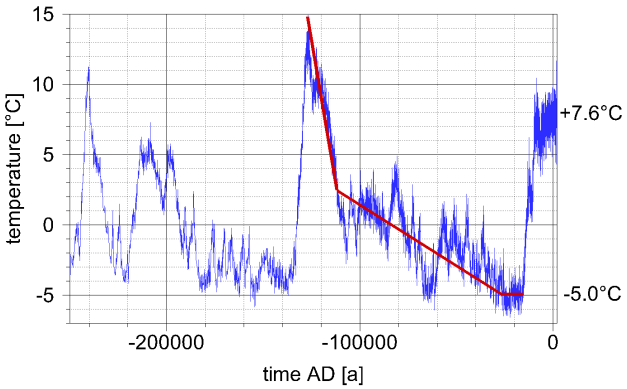

Figure 4. Adopted history of SAT over Germany; adopted data in blue, simplified curve in red.

The cooling/cold period of choice has been selected to be the interval between 127,000 and 15,500-years BC. For modelling purposes, the temperature evolution is smoothened to a polygon as indicated by the red line in Figure 4. It is also shifted in time for convenience according to Table 1.

Table 1. Simplified temperature evolution.

Real time [a BC]	Model time [a]	Temperature [°C]
127,000	0	14.80
111,600	15,400	2.45
26,600	100,400	-5.00
15,500	111,500	-5.00

The initial temperature field is calculated according to a geothermal gradient of 0.0232 °C/m where the initial temperature of 14.8 °C is assigned to the top of the model. Model calculations proved this to be consistent with the heat flux of 78 mW/m² over the bottom boundary.

It has to be noted that the effect of cyclic surface temperature variations discussed above with respect to daily and seasonal changes, applies in principle also to climate-caused fluctuations. Amplitude and frequency of these changes control the depth to which the thermal impact can be observed. The bottom of the model should thus extend beyond the zero amplitude. This is further discussed in section 2.3.2.

2.3 Modelling

2.3.1 Initial and boundary conditions

The whole set of hydraulic and thermal initial and boundary conditions is depicted in Figure 5 and subsequently discussed.

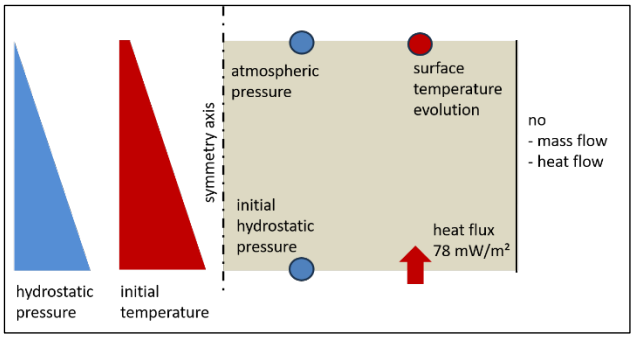

Figure 5. Hydraulic and thermal initial and boundary conditions.

As an initial condition, no groundwater flow is assumed in the model which implies a hydrostatic pressure distribution over the domain. The initial pressure distribution is generated using a hydraulic head of 0 m at the top of the model.

The lateral boundary of the axial symmetric domain is a no-flow boundary. It is expected that any influence of the lake on the freezing process can be neglected if this boundary is located sufficiently far from the lake. In this case the flow at the lateral boundary is strictly vertical and no mass exchange occurs across this boundary. The resulting model width is determined in section 2.3.2.

The pressure at the bottom boundary is fixed to the initial hydrostatic value of 19.54 MPa assuming a mean water density of 996 kg/m³. This introduces an error over time when phase change of water to ice occurs. The displacement of water due to volumetric expansion during ice formation results in lateral water migration across open model boundaries, thereby changing the weight of the water column and thus the hydraulic pressure at the bottom. Under these circumstances, a lateral no-flow boundary forces excess water out of the model through the top boundary where, in reality, the ice should impede water flow. The error from a fixed pressure at the bottom can only be limited maximizing the depth for the model domain. This is determined in section 2.3.2.

The lateral thermal boundary is assumed to be sufficiently far from the model axis that no temperature signal caused by the lake reaches the lateral boundary. In other words, the heat flux along this boundary is assumed to be strictly vertical so that no heat exchange across the boundary occurs.

2.3.2 Preparatory modelling

To prepare the final model, some preparatory modelling work was required. This included a) determining an appropriate model width and depth and b) checking for the

compliance of model temperatures and admissible temperature ranges for the EOS.

Tentative model runs indicate that lateral boundary should be arranged at a radial distance of 1000 m from the model axis to ensure a sound approximation of no flow and no heat flux across this boundary.

As discussed in subsection 2.3.1, the hydraulics require a maximized model depth. In order to ensure validity of the new EOS with respect to temperature and pressure, this depth is set to 2000 m. However, modelling by way of trial indicates that a temperature signal from the top reaches a depth of 2000 m in less than 10,000 years in this model. This is very little compared to the more than 111,500 years assessed in this study.

While further extensions of the formulations for the EOS for water would be rather hard to derive, the EOS for the rock are well-known up to a temperature of 200 °C (cf., Kröhn 2010). It is thus assumed here that exclusion of water in the pore space below a depth of 2000 m constitutes a reasonable approximation for heat transport at great depths. Different domains are consequently considered for hydraulic and for thermal processes. The domain for the hydraulic simulations remains as discussed above but the thermal model is extended downwards by an additional piece of solid rock material with zero porosity. Calculations with this enlarged model indicate that the temperature signal from the top does not reach a depth of 6000 m within 110,000 years. The undisturbed temperature at that depth is 157 °C attesting validity of the thermal EOS for rock in this model.

2.3.3 The final model

Based on the problem definition in section 2.1, the model shape described in section 2.2, and the remaining specifications from the previous subsection 2.3.2, a single model run has been performed to inspire confidence in the mathematical model and to assess the possible thermo-hydraulic conditions in the subsurface.

3 RESULTS

3.1 Simulation times of interest

Three points in time in this simulation appear to be of particular interest: (1) an early time to represent effects at the beginning of cooling, chosen to be 1000 years, (2) 60,000 years which is some time after the onset of freezing, and (3) the end of the cooling climate at 111,500 years. Results with respect to these times are presented in the following subsections.

3.1.1 1000 years: Effect of cooling

After 1000 years model time, the surface temperature has decreased from 14.8 to 14.0 °C. This relatively small difference increases the vertical temperature gradient to the extent that the heat flux over the granitic surface increases by a factor of about 2.5. The water in the lake, however, has a much lower thermal conductivity and thus shields the bottom of the lake from cooling. Heat flux from below is diverted around the lake as visualized in Figure 6 where heat flux is plotted as a vector field, as the related distribution of absolute velocity values highlighted in colour, and as a couple of pathlines. The resulting temperature field, given as isolines and a coloured scalar field in Figure 7 shows the resulting temperature anomaly of a few tenths °C around the lake.

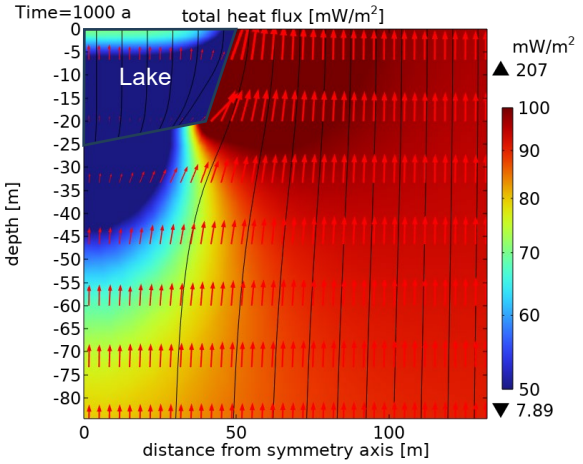

Figure 6. Total heat flux in the vicinity of the lake after 1000 years.

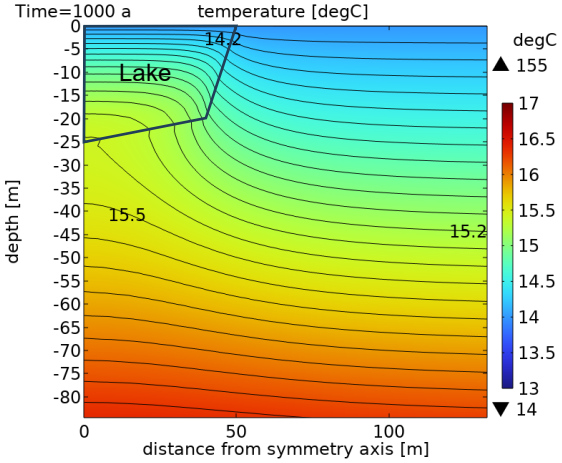

Figure 7. Temperature around the lake after 1000 years.

3.1.2 60,000 years: Effect of freezing

In the model, the surface temperature falls below 0 °C after about 43,400 years. After 60,000 years simulation time, ice can be found down to about 20 m depth. Since the model accounts for the volumetric increase of water due to freezing but does not allow for ice on the lake to heave, the remaining water in the lake gets squeezed out into the rock as illustrated in Figure 8 showing the scalar saturation field and qualitatively the velocity vectors for the water flow.

The absolute flow velocity depicted for a large part of the model in Figure 9 is quite small, less than 10^{-12} m². It is consistent, though, with the slow downward progress of the ice front because forming of ice results in volumetric expansion and leads to a downwards directed displacement of water.

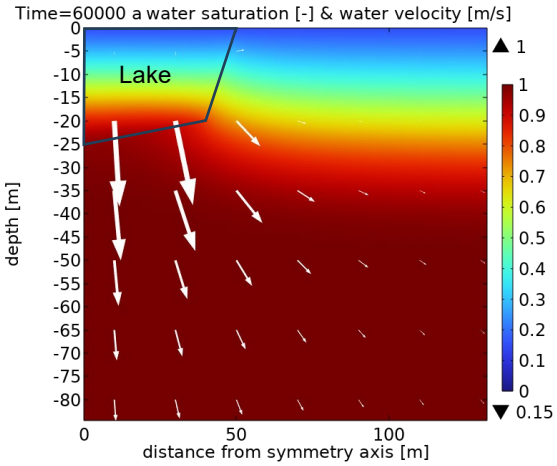

Figure 8. Liquid water saturation and water velocity in the vicinity of the lake after 60,000 years.

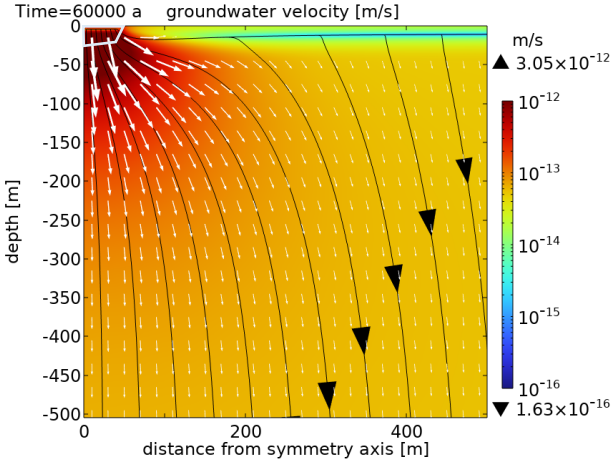

Figure 9. Water flow after 60,000 years.

3.1.3 111,500 years: End of cold age

The end of the cold age considered here is reached after 111,500 a. The model calculates a thickness of the frozen ground of about 150 m (see Figure 10). The freezing front becomes horizontal as the effect of the lake is no longer felt.

As the thermal conductivity for ice is lower than for the rock (but higher than for water), the frozen lake still forms an impediment for heat flow even if not as effective as the water at the beginning of the simulated cold age. The temperature anomaly around the lake at the end of the simulation (see Figure 11) is thus a permanent feature.

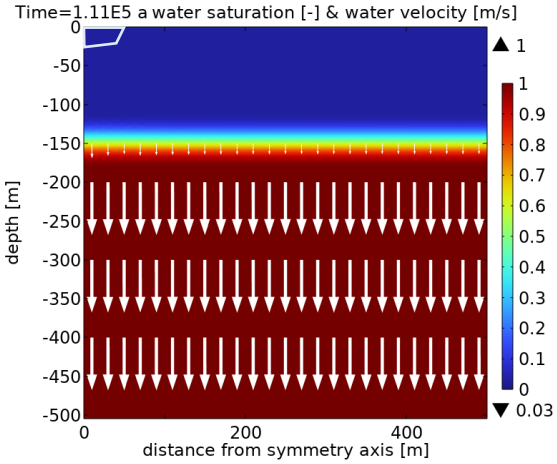

Figure 10. Water saturation and water velocity after 111,500 years.

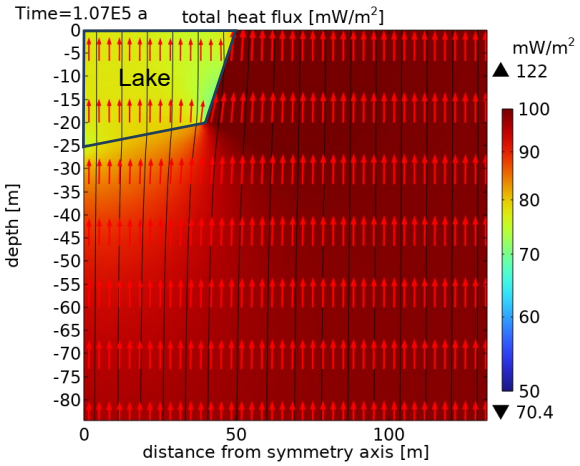

Figure 11. Total heat flux in the vicinity of the lake after 111,500 years.

3.2 Evolution of water density

The interplay of increasing temperature and hydraulic pressure with depth results in a peculiar evolution of the vertical water density distribution. While the density at the top varies only by about 1 kg/m³, it differs by 5 kg/m³ at 2000 m depth. Furthermore, the maximum water density of 999.1 kg/m³ is initially located at a depth of about 100 m but increases to 1002.3 kg/m³ and moves down to 700 m depth after 111,500 years model time (see Figure 12).

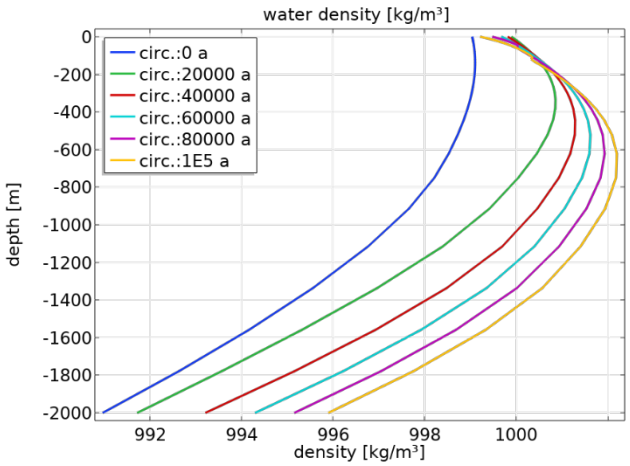

Figure 12. Evolution of the water density with depth.

4 Discussion

The first attempt to reproduce talik formation during a change to colder climates has failed. However, modelling has led to reasonable results. There is a temperature anomaly in the vicinity of the lake because the lake is shielding the ground below to a certain extent from heat loss due to its comparatively low thermal conductivity. This feature is visible over the whole simulated time and should still be visible when equilibrium of heat flow according to the thermal boundary conditions is reached.

Groundwater flow is basically driven by the freezing of water as the less dense ice displaces the remaining water due to expansion during phase change. The resulting flow velocity is very low, lying in the range of µm/a and therefore far too low to provoke heat convection. Under these circumstances, even the temperature- and pressure-dependent water density and viscosity are not sufficient to start any sort of heat convection. Thus, by and large, heat flow is restricted to conduction in this model.

Squeezing water from the lake due to the volumetric expansion during freezing is the result of having a geometrically fixed top boundary that forces the newly formed ice downwards. This is of course unrealistic as the ice would be floating on top of the lake water — at least for quite some time — and thus exerting less pressure on the lake water. In a more realistic treatment of the lake, the effect of squeezing water out under the lake ice would therefore be much less pronounced. As a result, the progress of the ice front with time would be even less disturbed by the lake and the ice front would be even less deviating from a horizontal course. However, it would also put up less resistance against a hypothetical rising of warmer water from under the lake.

5 Conclusions and Outlook

A realistic numerical model for groundwater flow under permafrost conditions has been presented. While the main goal to track talik forming numerically has been missed, the otherwise reasonable modelling results encourage further systematic investigations. A large number of model cases remain to be considered, checking for the impact of additional features such as:

- a non-horizontal groundwater table,
- higher permeability and porosity of the rock,
- varying the heat flux from the inner earth,
- seasonal temperature variations,
- a better representation of the lake in the model,
- heterogeneities in the rock, or
- the influence of a deep aquifer.

6 Acknowledgements

Funding by the Federal Ministry for Economic Affairs and Energy (BMWi) and the Federal Ministry for the Environment, Nature Conservation, Nuclear Safety and Consumer Protection BMUV under contract numbers 02 E 11809A (project HYMNE) and 02 E 11941 (project WiGru-9) are gratefully acknowledged.

7 References

Burn, C.R. 2020. 'Permafrost Landscape Features', in *Encyclopedia of the World's Biome,* Vol. 2, pp. 303–320. Available at: https://doi.org/10.1016/B978-0-12-409548-9.12423-6.

Delisle, G. 1998. 'Numerical simulation of permafrost growth and decay', *Journal of Quaternary Science* 13(4), pp. 325–333.

Deutscher Bundestag 2017. *Gesetz zur Suche und Auswahl eines Standortes für ein Endlager für hochradioaktive Abfälle (Standortauswahlgesetz - StandAG)*, decision of the Deutscher Bundestag.

Deutscher Wetterdienst (DWD) 2012. *Klimastatusbericht Deutschland, Jahr 2011*, Deutscher Wetterdienst, Selbstverlag.

Deutscher Wetterdienst (DWD) 2021. *Klimastatusbericht Deutschland, Jahr 2020*, Deutscher Wetterdienst, Selbstverlag.

Deutscher Wetterdienst (DWD) 2023. *CDC – Climate Data Center, annual air temperature over Germany*. Available at: https://opendata.dwd.de/climate_environment/CDC/regional_averages_DE/annual/air_temperature_mean/regional_averages_tm_year.txt.

Dye, S.T. 2012. 'Geoneutrinos and the radioactive power of the Earth', *Reviews of Geophysics* 50(3). Available at: https://doi.org/10.1029/2012RG000400.

Gens, A., Guimaraes, L. do N., Garcia-Molina, A., and Alonso, E.E. 2002. 'Factors controlling rock–clay buffer interaction in a radioactive waste repository', *Engineering Geology* 64, pp. 297–308.

ERIH (European Route of Industrial Heritage) 2023. *Industrial history of European countries*. Available at: https://www.erih.net/how-it-started/industrial-history-of-european-countries.

Fuchs, S., Förster, A., and Norden, B. 2022a. 'Evaluation of the terrestrial heat flow in Germany: A case study for the reassessment of global continental heat-flow data', *Earth-Science Reviews* 235(2022), 104231. Available at: https://doi.org/10.1016/j.earscirev.2022.104231.

Fuchs, S., Norden, B., and Förster, A., 2022b. 'The German Heat Flow Database 2022', *GFZ Data Services*. Available at: https://doi.org/10.5880/GFZ.4.8.2022.015.

Harper, J., Hubbard A., Ruskeeniemi, T., Claesson Liljedahl, L., Lehtinen, A., Booth, A., et al. 2011. 'The Greenland Analogue Project, Yearly Report 2010', *Svensk Kärnbränslehantering AB* Report R-11-23, Stockholm.

IAPWS (International Association for the Properties of Water and Steam) 2003. *Revised Release on the IAPS Formulation 1985 for the Viscosity of Ordinary Water Substance*. Available at: http://www.iapws.org.

IAPWS (International Association for the Properties of Water and Steam) 2008. *Revised Release on the IAPWS Formulation 2008 for the Viscosity of Ordinary Water Substance*. Available at: http://www.iapws.org.

IAPWS (International Association for the Properties of Water and Steam) 2011. *Revised Release on the IAPWS Formulation 2011 for the Thermal Conductivity of Ordinary Water Substance*. Available at: http://www.iapws.org.

IAPWS (International Association for the Properties of Water and Steam) 2015. *Revised Guideline on Thermodynamic Properties of Supercooled Water*. Available at: http://www.iapws.org.

Johansson, E. 2016. *The influence of climate and permafrost on catchment hydrology*. Doctoral Thesis, Department of Physical Geography, Stockholm University.

Johansson, E., Gustafsson, L.-G., Berglund, S., Lindborg, T., Selroos, J.-O., Claesson Liljedahl, L., and Destouni, G. 2015. 'Data evaluation and numerical modeling of hydrological interactions between active layer, lake and talik in a permafrost catchment, Western Greenland', *Journal of Hydrology* 36. doi:10.1016/j.jhydrol.2015.05.026.

Jouzel, J. and Masson-Delmotte, V. 2007. 'EPICA Dome C Ice Core 800KYr deuterium data and temperature estimates', *PANGAEA*. Available at: https://doi.org/10.1594/PANGAEA.683655.

Keller, S. 1998. 'Permafrost in der Weichsel-Kaltzeit und Langzeitprognose der hydrogeologischen Entwicklung der Umgebung von Gorleben/NW Deutschland', Zeitschrift für Angewandte Geologie 44(2), pp. 111–119.

Kröhn, K.-P. 2010. 'State Variables for Modelling Thermohaline Flow in Rocks', *Gesellschaft für Anlagen- und Reaktorsicherheit (GRS) mbH* report GRS-268. Köln.

Kröhn, K.-P. 2022. Basics for groundwater flow under permafrost conditions in the context of radioactive storage', *Gesellschaft für Anlagen- und Reaktor-sicherheit (GRS) gGmbH* report GRS-707. Braunschweig.

Kröhn, K.-P. 2023. 'Investigations On Talik Formation During Changes To Cold Climates', in *COMSOL Conference 2023*. Munich, Germany.

Leshchinsky, D. and Perry, E.B. 1987. 'A Design Procedure for Geotextile Reinforced Walls', in *Geosynthetics '87*. New Orleans, Louisiana, United States: pp. 95–107.

Loyd, S., Becker, T., Conrad, C., Lithgow-Bertelloni, C., and Corsetti, F. 2007. 'Time variability in Cenozoic reconstructions of mantle heat flow: Plate tectonic cycles and implications for Earth's thermal evolution', *Earth, Atomospheric, and Planetary Sciences* 104(36), pp. 14266–14271. doi:10.1073/pnas.0706667104.

Mackay, J.R. 1962. 'Pingos of the Pleistocene Mackenzie Delta area', *Geographical Bulletin*, pp. 21–63.

Parazoo, N.C., Koven, C.D., Lawrence, D.M., Romanovsky, V., and Miller, C.E. 2018. 'Detecting the permafrost carbon feedback: talik formation and increased cold-season respiration as precursors to sink-to-source transitions', *The Cryosphere* 12, pp. 123–144. Available at: https://doi.org/10.5194/tc-12-123-2018.

Renssen, H. and Vandenberghe, J. 2003. 'Investigation of the relationship between permafrost distribution in NW Europe and extensive winter sea-ice cover in the North Atlantic Ocean during the cold phases of the Last Glaciation', *Quaternary Science Reviews* 22, pp, 209–223.

Solomon, S., Qin, D., Manning, M., Marquis, M., Averyt, K., Tignor, M.M.B., Miller, H.L. jr., and Chen, Z. (eds.) 2007. *Climate Change 2007 - The Physical Science Basis*. Contribution of Working Group I to the Fourth Assessment Report of the Intergovernmental Panel on Climate Change. New York, New York, United States: Cambridge University Press,

Svensk Kärnbränslehantering AB (SKB) 2006. *Climate and climate-related issues for the safety assessment SR-Can.* SKB, Technical report TR-06-23, Stockholm.

van Everdingen, R.O. 2005. 'Multi-language glossary of permafrost and related ground-ice terms', *International Permafrost Association*. Available at: Glossary_of_Permafrost_and_Ground-Ice_IPA_2005.pdf.

Vandenberghe, J. and Pissart, A. 1993. 'Permafrost changes in Europe during the Last Glacial', *Permafrost and Periglacial Processes* 4, pp. 121–135.

APPENDIX A: DESCRIPTION OF MODEL BASICS

The indices w, I, and m stand for water, ice and matrix.
(for more details see Kröhn (2022) and Kröhn (2023))

A.1 Processes

- Advective water flow
- Sinks/sources for water (not used here)
- Sinks/sources of mass of water and ice due to phase changes; concurrent volumetric changes
- Heat convection and conduction
- Hydromechanical heat dispersion (not used here)
- Sinks/sources for heat (not used here)
- Release/consumption of latent heat

A.2 Assumptions

- Three phases considered: water, ice, and rock
- No movement of ice or rock
- Constant porosity
- Generalized Darcy flow including
  - Soil Freezing Characteristic Curve (SFCC)
  - Relative permeability dependent on the SFCC
- Local thermal equilibrium
- Fourier's law
- Isotropic thermal conductivity
- All EOS depend on temperature; EOS for water also on pressure
- No boiling

A.3 Balance equations

A.3.1 Mass balance

$$-\nabla\cdot\left(\rho_w\frac{k_{rw}}{\eta_w}\boldsymbol{k}\cdot(\boldsymbol{\nabla}p_w-\rho_w\boldsymbol{g})\right)=$$

$$\rho_w\,q_w-\left[\Phi\left(\rho_w-\rho_i\right)\frac{\partial S_w}{\partial T}+S_w\Phi\frac{\partial\rho_w}{\partial T}\right]\frac{\partial T}{\partial t} \qquad \text{[A.1]}$$

ρ	-	density
η	-	viscosity
k	-	permeability
k_r	-	relative permeability
p	-	pressure
g	-	gravitational acceleration
q	-	volumetric source
Φ	-	porosity
S	-	saturation
T	-	temperature
t	-	time

A.3.2 Energy balance

$$\left(\begin{array}{c}S_w\Phi\rho_w\left[T\frac{\partial c_{s\,w}}{\partial T}+c_{s\,w}\right]+S_i\Phi\rho_i\left[T\frac{\partial c_{s\,i}}{\partial T}+c_{s\,i}\right]\\+(1-\Phi)\rho_m\left[T\frac{\partial c_{s\,m}}{\partial T}+c_{s\,m}\right]-L\rho_i\Phi\frac{\partial S_i}{\partial T}\end{array}\right)\frac{\partial T}{\partial t}$$

$$+(\boldsymbol{v_{a\,w}}S_w\rho_w\Phi)\cdot\boldsymbol{\nabla}(c_{s\,w}T)$$

$$-\nabla\cdot[(S_w\Phi\,\boldsymbol{\lambda_w}+S_i\Phi\,\boldsymbol{\lambda_i}+(1-\Phi)\,\boldsymbol{\lambda_m}+S_w\Phi c_{s\,w}\rho_w\boldsymbol{D_w})\cdot\boldsymbol{\nabla}T]$$

$$=r_{hQ}+c_{s\,w}\;\rho_w\,q_w\left(T_w-\dot{T}\right)+S_w\Phi\rho_wT\frac{\partial c_{sw}}{\partial p}\frac{\partial p}{\partial t} \qquad \text{[A.2]}$$

c_s	-	specific heat
L	-	latent heat
v_a	-	interstitial velocity
λ	-	thermal conductivity
D	-	hydrodynamic dispersion
r_{hQ}	-	source term for directly applied heat
$\dot{T}$	-	temperature of inflowing water

A.4 Constitutive equations

A.4.1 Equations

$$\boldsymbol{v_{a\,w}}=\boldsymbol{v_{a\,w}}\left(\boldsymbol{v_{f\,w}}\left(k_{rw}(S_w(T))\right),S_w(T),\Phi,g,\rho_w,\eta_w,p_w\right)$$

$$S_w=S_w(T)$$

$$k_{rw}=k_{rw}(S_w(T))$$

$$\boldsymbol{J_{cond\,j}}=\boldsymbol{J_{cond\,j}}(S_j(T),\Phi,\lambda_j,T),\ \mathrm{j}=\mathrm{w,i,m}$$

$$\boldsymbol{J_{disp\,w}}=\boldsymbol{J_{disp\,w}}(S_w(T),\Phi,\boldsymbol{D_w}(\boldsymbol{v_{a\,w}},\alpha_l,\alpha_t),c_{s\,w},\rho_w,T)$$

A.4.2 Parameters

$$\Phi,\mathrm{g}=const.$$

$$\eta_w=\eta_w(p_w,T)$$

$$\lambda_w=\lambda_w(p_w,T)\quad\lambda_i=\lambda_i(T)\quad\lambda_m=\lambda_m(T)$$

A.5 Equations of state

$$\rho_w=\rho_w(p_w,T)\quad\rho_i=const.\quad\rho_m=const.$$

$$c_{sw}=c_{sw}(p_w,T)\quad c_{si}=c_{si}(T)\quad c_{sm}=c_{sm}(T)$$